



1 Characterization of urban amine-containing particles in Southwestern China: seasonal  
2 variation, source, and processing

3 Yang Chen<sup>1,2\*</sup>, Mi Tian<sup>1</sup>, Rujin Huang<sup>2</sup>, Guangming Shi<sup>4</sup>, Huanbo Wang<sup>1</sup>, Chao Peng<sup>1</sup>,  
4 Junji Cao<sup>2</sup>, Qiyuan Wang<sup>2</sup>, Shumin Zhang<sup>3</sup>, Dongmei Guo<sup>3</sup>, Leiming Zhang<sup>5</sup>, and Fumo  
5 Yang<sup>1,4,\*</sup>

6 <sup>1</sup>Research Center for Atmospheric Environment, Chongqing Institute of Green and  
7 Intelligent Technology, Chinese Academy of Sciences, Chongqing 400714, China.

8 <sup>2</sup>Key Lab of Aerosol Chemistry & Physics, State Key Laboratory of Loess and Quaternary  
9 Geology, Institute of Earth Environment, Chinese Academy of Sciences, Xi'an 710061,  
10 China.

11 <sup>3</sup>School of Basic Medical Sciences, North Sichuan Medical College, Nanchong 637000,  
12 Sichuan, China.

13 <sup>4</sup>College of Architecture and Environment, Sichuan University, Chengdu 610065, China

14 <sup>5</sup>Air Quality Research Division, Science and Technology Branch, Environment and  
15 Climate Change Canada, Toronto M3H 5T4, Canada

16 Correspondence to: Yang Chen ([chenyang@cigit.ac.cn](mailto:chenyang@cigit.ac.cn)); Fumo Yang ([fmyang@cigit.ac.cn](mailto:fmyang@cigit.ac.cn))

17 Keyword: single particle; amine; urban environment, processing

18



19           **Abstract**

20    Amine-containing particles were characterized in an urban area of Chongqing during both  
21    summer and winter using a single particle aerosol mass spectrometer (SPAMS). Among  
22    the collected ambient particles, 12.7% were amine-containing in winter and 8.3% in  
23    summer. Amines were observed to internally mix with elemental carbon (EC), organic  
24    carbon (OC), sulfate, and nitrate. Diethylamine (DEA) was the most abundant in both  
25    number and peak area among amine-containing particles. Wintertime amine-containing  
26    particles were mainly from the northwest direction where a forest park was located; in  
27    summer, they were from the northwest and southwest (traffic hub) directions. These origins  
28    suggest that vegetation and traffic were the primary sources of particulate amines. The  
29    average relative peak area of DEA depended strongly on humidity, indicating that the  
30    enhancement of DEA was possibly due to increasing aerosol water content and aerosol  
31    acidity. Using an adaptive resonance theory neural network (ART-2a) algorithm, four  
32    major types of amine-containing particles were clustered including amine-organic-carbon  
33    (A-OC), A-OCEC, DEA-OC, and A-OCEC-aged. The identified particle types imply that  
34    amine was uptaken by particles produced from traffic and biomass burning. Knowledge  
35    gained in this study is helpful to understand the atmospheric processing, origin, and sources  
36    of amine-containing particles in the urban area of Chongqing.



## 37      **1. Introduction**

38      Amines are ubiquitous in the atmosphere and have both natural (ocean, biomass burning,  
39      and vegetation) and anthropogenic (animal husbandry, industry, combustion, traffic)  
40      emission sources (Ge et al., 2011a). Trimethylamine (TMA) is one of the most abundant  
41      amines with an estimated global emission flux of  $170\text{Gg year}^{-1}$  (Ge et al., 2011a). Amines  
42      in the gas phase compete with ammonia in acid-base reactions, participate in the gas-  
43      particle partitioning, and contribute to wet and dry deposition (Angelino et al., 2001;  
44      Monks, 2005; Gómez Alvarez et al., 2007; De Haan et al., 2011; Huang et al., 2012; You  
45      et al., 2014). Gaseous amines also play an essential role in new particle formation via  
46      enhancing the ternary nucleation of the sulfuric acid clusters in remote areas (Bzdek et al.,  
47      2012; Kirkby et al., 2011). Recently, Yao et al. (2018) revealed that  $\text{H}_2\text{SO}_4$ -diethylamine  
48      (DMA)-water clusters were important during the new particle formation events in polluted  
49      urban areas. Amines are also essential in the growth of ambient particles. For example,  
50      particulate aminium salts, which were produced via amine-acid neutralization, tended to  
51      prevent the coagulation between pre-existing particles thus enhanced the particle number  
52      concentration (Wang et al., 2010; Smith et al., 2010). Moreover, the enhancement of TMA  
53      has been found during cloud and fog processing ((Zhang et al., 2012; Rehbein et al., 2011).  
54      Understanding mixing state of amine-containing particles is important to understand their  
55      processing and impact.

56      Single particle mass spectrometers (SPMS), such as aerosol time-of-flight mass  
57      spectrometer (ATOFMS) and Single Particle Aerosol Mass Spectrometer (SPAMS), have  
58      been used in real-time measuring amine-containing particles for chemical composition and



59 mixing state. The term SPAMS is different from the Aerodyne soot-particle aerosol mass  
60 spectrometer (SP-AMS) which is a kind of aerosol mass spectrometer (AMS), detecting  
61 the mass concentrations of black carbon, sulfate, nitrate, ammonium, chloride, and organics  
62 (Onasch et al., 2012; Wang et al., 2016). The chemical composition and mixing state of  
63 TMA-containing particles have been reported worldwide, such as in North America  
64 (California, USA (Denkenberger et al., 2007; Qin et al., 2012)); Ontario, Canada (Tan et  
65 al., 2002; Rehbein et al., 2011); Mexico City (Moffet et al., 2008)); Europe (Barcelona,  
66 Cork, Zurich, Paris, Dunkirk and Corsica (Healy et al., 2015; Dall'Osto et al., 2016)), and  
67 China (Guangzhou, Shanghai and Xi'an (Zhang et al., 2012; Chen et al., 2016; Huang et  
68 al., 2012)). Chemical composition and mixing state of amine-containing particles varied in  
69 these locations. Thus the location-specific studies are still necessary.

70 Knowledge of amine-containing particles is limited in southwestern China. In this region,  
71 Chongqing is a megacity with a population of 8.23 million and on the edge of the Sichuan  
72 Basin. It is a subtropical, industrial, and polluted city (Chen et al., 2017b; Tao et al., 2017).  
73 Fog events frequently occurred in this area, and the city is known as the “fog city” in China.  
74 How high relative humidity (RH) affects the atmospheric processing of amine-containing  
75 particles needs investigation. This study aims to characterize the amine-containing  
76 particles, including chemical composition, mixing state, atmospheric processing, and  
77 source in Chongqing during winter and summer.

78



79      **2. Methods**

80      **2.1 Sampling site**

81      Ambient single particles were collected at an urban air quality supersite from 07/05/2016  
82      to 08/14/2016 (referred to as a summer season) and from 01/21/2016 to 02/25/2016  
83      (referred to as a winter season). The supersite has been described in our previous studies  
84      (Chen et al., 2017a; Chen et al., 2017b). Briefly, the supersite is located on the roof of a  
85      commercial office building (106.51°E, 29.62°N) with a height of 30 m above the ground.  
86      The building is surrounded by business and residential communities, 15 km away from the  
87      city center. A forest park, with an area of 3 km<sup>2</sup>, is located in the northwest of the sampling  
88      site and a traffic hub in the southwest.

89      **2.2 Instrumentation**

90      A SPAMS was deployed for single particle sampling, and the technical description of the  
91      instrument is available in literature (Li et al., 2011; Chen et al., 2017b). Briefly, after  
92      passing through a diffusive dryer, particles in a size range of 0.1–2.0 μm are sampled via  
93      an aerodynamic lens and form a particle beam. Particles in the beam cross two pre-  
94      positioned laser beams (Nd: YAG, 532 nm) one-by-one, and the vacuum aerodynamic  
95      diameter ( $D_{va}$ ) of each particle is determined via its time-of-flight. Particles are ionized  
96      using an Nd: YAG laser operating at a wavelength of 266 nm. The yielding ions are  
97      analyzed using a bipolar time-of-flight mass spectrometer. Due to the limitation of SPAMS,  
98      quantification of amines was not attempted.

99



### 100      **2.3 Data analysis**

101      The SPAMS data were imported into the YAADA toolkit (Software Toolkit to Analyze  
102      Single-Particle Mass Spectral Data, v 2.11) to form a particle dataset. The analysis was  
103      conducted using the marker ions of amines.:  $m/z$  59  $[(\text{CH}_3)_3\text{N}]^+$  (TMA), 74  $[(\text{C}_2\text{H}_5)_2\text{NH}_2]^+$   
104      (diethylamine, DEA), 86  $[(\text{C}_2\text{H}_5)_2\text{NCH}_2]^+$  or  $[\text{C}_3\text{H}_7\text{NHC}_2\text{H}_4]^+$  (DEA or DPA), 101  
105       $[(\text{C}_2\text{H}_5)_3\text{N}]^+$  (TEA), 102  $[(\text{C}_3\text{H}_7)_2\text{NH}_2]^+$  (DPA), 114  $[(\text{C}_3\text{H}_7)_2\text{NCH}_2]^+$  (DPA), and 143  
106       $[(\text{C}_3\text{H}_7)_3\text{N}]^+$  (TPA) (Healy et al., 2015). Firstly,  $m/z$  59 was used for querying the TMA-  
107      containing particles;  $m/z$  74 for the DEA-containing particles and  $m/z$  86 for TEA-  
108      containing particles, and so on. After the duplicated particles in the query results being  
109      removed, these results were combined into an amine-containing particle cluster. Various  
110      amines could be both internally and externally mixed in these particle clusters.

111      An adaptive resonance theory based neural network algorithm (ART-2a) was applied to  
112      cluster the amine-containing particle types using a vigilance factor of 0.70, a learning rate  
113      of 0.05, and 20 iterations (Song et al., 1999). This procedure produced 67 clusters in  
114      summer and 75 clusters in winter; many of these clusters exhibited identical mass spectra  
115      with slight differences in specific ion peak areas. A well-established combining strategy,  
116      on the basis of similar mass spectra, temporal trends, and size distribution, was adopted to  
117      merge these particle clusters into the final particle types (Dallosto and Harrison, 2006).

118      Polar plot can gain an impression of the graphical distributions of potential sources  
119      influencing the measurement site. It presents concentration data of pollutants that vary by  
120      wind speed and wind direction (Carslaw et al., 2006).



121        **3. Results and discussion**

122        **3.1 Single particle chemical composition and seasonal variation**

123        Amine-containing particles were 12.7% in winter SPAMS dataset and 8.3% in the summer  
124        one. The DEA-containing particles were dominant among the total amine-containing  
125        particles, accounting for 70% and 78% in winter and summer, respectively, while TMA-  
126        containing particles were a minor group, accounting for up to 7% in winter and 3% in  
127        summer. The average mass spectra of DEA-, DPA, and TMA-containing particles are  
128        provided in Figure S1. All three mass spectra showed strong homogeneity. The  
129        determination coefficient ( $R^2$ ) between DEA- and DPA- containing particles were 0.98,  
130        and  $R^2$  between DEA- and TMA- containing particles was 0.83.

131        Figure 1 shows the digital mass spectra of amine-containing particles in two seasons. The  
132        assignment of ions is shown in Table 1. In both seasons, the dominant ions were  $K^+$  ( $m/z$   
133        39 and 41), amines ( $m/z$  59, 74, and 86), and organics ( $m/z$  43, 51, 63, and 77). The mixing  
134        ratios of ammonium ( $NH_4^+$ ,  $m/z$  18) and polycyclic aromatic hydrocarbons (PAHs e.g.,  
135         $m/z$  116 ( $[C_9H_8]^+$ ), 129 ( $[C_{10}H_9]^+$ ), 140 ( $[C_{11}H_8]^+$ ), and 153 ( $[C_{12}H_9]^+$ )) were higher in  
136        winter than in summer. The strong signal of  $NH_4^+$  was possibly due to the lower  
137        temperature ( $8^\circ C$ ) in winter than in summer ( $31^\circ C$ ). The mixing ratios of  $m/z$  59 were 0.45  
138        and 0.44 during summer and winter, respectively.

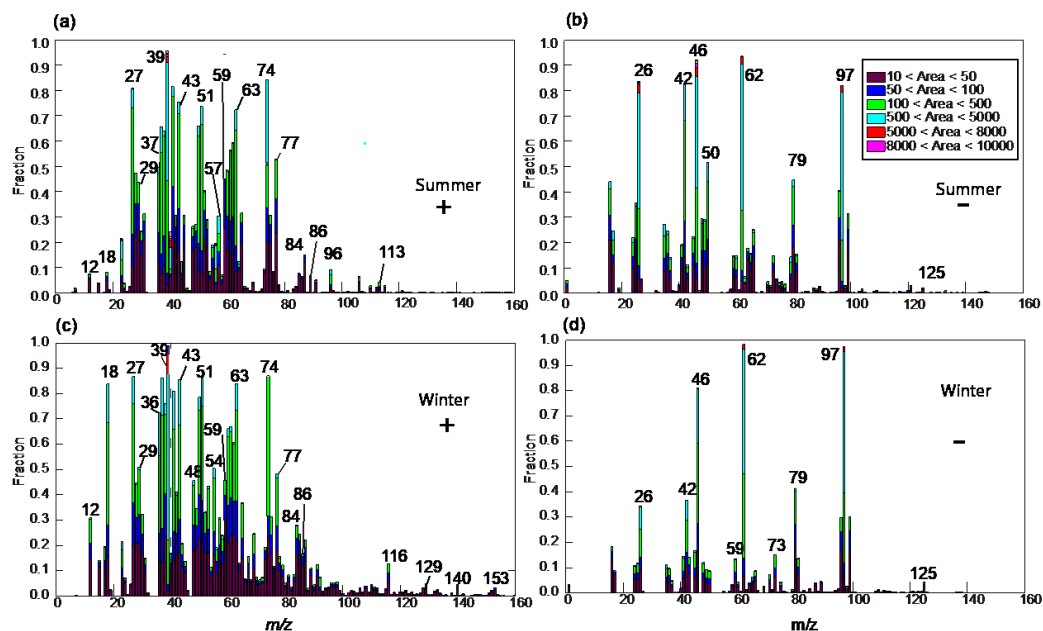
139        In the negative mass spectra of two seasons (Figures 1(b) and 1(d)), the dominating ions  
140        were  $CN^-$  ( $m/z$  -26),  $CNO^-$  ( $m/z$  -42), nitrate ( $m/z$  -46 and -62), phosphate (-79), and  
141        sulfate ( $m/z$  -80 and -97). Primary species, such as  $CN^-$  and  $CNO^-$  were commonly from



142 biomass burning (BB) and organonitrogen (Pratt et al., 2011). Levoglucosan markers from  
143 BB, such as  $-45$ ,  $-59$ , and  $-71$  were also detected. Dust markers, such as  $[\text{SiO}_2]^-$  ( $m/z -$   
144  $60$ ),  $[\text{}^{28}\text{SiO}_3]^-$  or  $[\text{AlO}_2(\text{OH})]^-$  ( $-76$ ), and  $[\text{PO}_3]^-$ , were also detected during summertime,  
145 suggesting the influence of dust particles.

146 Seasonal variations of chemical composition and unscaled size distribution are available in  
147 supporting information. The average peak area of each ion was normalized in both summer  
148 and winter, and the normalized values of each  $m/z$  in winter were used to subtract the  
149 summer ones to generate a subtraction plot (Figure S2 (Qin et al., 2012)). A positive value  
150 suggests that it is more predominant in summer, otherwise in winter. Nitrate was more  
151 abundant in winter than summer.  $\text{Ca}^+$  ( $m/z$  40) and  $\text{Fe}^+$  ( $m/z$  56) were more prevalent during  
152 summer. Organic species, such as  $\text{C}_2\text{H}_3^+$  ( $m/z$  27),  $\text{C}_4\text{H}_3^+$  ( $m/z$  51),  $\text{C}_5\text{H}_3^+$  ( $m/z$  63), and  
153  $\text{C}_6\text{H}_5^+$  ( $m/z$  77) typically from aromatic hydrocarbons, were more predominant in summer.  
154 During wintertime, signals of sulfate ( $m/z -97$ ),  $\text{NO}_3^-$  ( $m/z -62$ ),  $\text{NH}_4^+$  ( $m/z$  18), and  $\text{K}^+$   
155 ( $m/z$  39) were more prominent than in summer, suggesting that the wintertime particles  
156 contained more secondary species. The unscaled size distribution of amine-containing  
157 particles also showed strong seasonal variations (Figure S3). Generally, amine-containing  
158 particles had monomodal size distributions in the droplet mode; and the distributions  
159 peaked at a larger  $D_{\text{va}}$  in summer than winter. For example, DEA-containing particles  
160 peaked at  $0.6 \mu\text{m}$  in winter and  $0.8 \mu\text{m}$  in summer, and DPA-containing particles at  $0.7 \mu\text{m}$   
161 in winter and  $0.9 \mu\text{m}$  in summer. The size distributions of the major amine-containing  
162 particles suggested that these particles had undergone substantial aging processes.





163

164 Figure 1. (a) and (c): the positive digital mass spectrum of amine-containing particles  
165 during summer and wintertime, respectively; (b) and (d): the negative digital mass  
166 spectrum during summer and wintertime, respectively. The ion height indicates its fraction  
167 in the amine-containing particle dataset, and the stacked color map suggested the ion peak  
168 area range.



169 Table 1. Assignment for ions in the mass spectra of amine-containing particles

m/z	Ion assignment	m/z	Ion assignment
+12	C <sup>+</sup>	-16	O <sup>-</sup>
+18	[NH <sub>4</sub> ] <sup>+</sup>	-17	[OH] <sup>-</sup>
+23	Na <sup>+</sup>	-26	[CN] <sup>-</sup>
+24	Mg <sup>+</sup>	-35	<sup>35</sup> Cl <sup>-</sup>
+27	Al <sup>+</sup> /[C <sub>2</sub> H <sub>3</sub> O] <sup>+</sup>	-37	<sup>37</sup> Cl <sup>-</sup>
+27	[CH <sub>3</sub> N] <sup>+</sup> / [C <sub>2</sub> H <sub>3</sub> ] <sup>+</sup>	-42	[CNO] <sup>-</sup>
+30	NO <sup>+</sup>	-43	[AlO] <sup>-</sup>
+39	<sup>39</sup> K <sup>+</sup>	-46	[NO <sub>2</sub> ] <sup>-</sup>
+40	Ca <sup>+</sup>	-48	[SO] <sup>-</sup>
+41	<sup>41</sup> K <sup>+</sup>	-50	[C <sub>4</sub> H <sub>2</sub> ] <sup>+</sup>
+43	[C <sub>2</sub> H <sub>3</sub> O] <sup>+</sup>	-60	[AlO(OH)] <sup>-</sup> or [SiO <sub>2</sub> ] <sup>-</sup>
+48	Ti <sup>+</sup>	-62	[NO <sub>3</sub> ] <sup>-</sup>
+51	C <sub>4</sub> H <sub>3</sub> <sup>+</sup>	-63	[PO <sub>2</sub> ] <sup>-</sup>
+54	<sup>54</sup> Fe <sup>+</sup>	-64	[SO <sub>2</sub> ] <sup>-</sup>
+57	<sup>57</sup> Fe <sup>+</sup> or [CaOH] <sup>+</sup>	-73	[C <sub>3</sub> H <sub>5</sub> O <sub>2</sub> ] <sup>-</sup>
+59	[(CH <sub>3</sub> ) <sub>3</sub> N] <sup>+</sup>	-76	[ <sup>28</sup> SiO <sub>3</sub> ] <sup>-</sup> or [AlO <sub>2</sub> (OH)] <sup>-</sup>
+63	[C <sub>3</sub> H <sub>3</sub> ] <sup>+</sup>	-77	[ <sup>28</sup> SiO <sub>3</sub> ] <sup>-</sup> or [H <sup>28</sup> SiO <sub>3</sub> ] <sup>-</sup>
+74	[(C <sub>2</sub> H <sub>5</sub> ) <sub>2</sub> NH <sub>2</sub> ] <sup>+</sup>	-79	[PO <sub>3</sub> ] <sup>-</sup>
+77	[C <sub>6</sub> H <sub>3</sub> ] <sup>+</sup>	-80	[SO <sub>3</sub> ] <sup>-</sup>
+113	[(CaO) <sub>2</sub> H] <sup>+</sup>	-88	[Si <sub>2</sub> O <sub>2</sub> ] <sup>-</sup> or [FeO <sub>2</sub> ] <sup>-</sup>
+116	[C <sub>9</sub> H <sub>8</sub> ] <sup>+</sup>	-97	[HSO <sub>4</sub> ] <sup>-</sup>
+129	[C <sub>10</sub> H <sub>9</sub> ] <sup>+</sup>	-125	H[NO <sub>3</sub> ] <sub>2</sub> <sup>-</sup>
+140	[C <sub>11</sub> H <sub>8</sub> ] <sup>+</sup>		
+153	[C <sub>12</sub> H <sub>9</sub> ] <sup>+</sup>		



### 170 3.2 Temporal trend, diurnal pattern, and origin of amine-containing particles

171 Figure 2 shows the temporal trends of RH, temperature, number count, and peak area of  
172 amine-containing particles. The winter temperature was lower ( $8.0 \pm 4.0$  °C) than summer  
173 ( $31 \pm 4$  °C), and RH was slightly higher ( $70 \pm 14\%$  versus  $64 \pm 16\%$ ) (Table 2). Stagnant air  
174 conditions existed in both seasons due to the low wind speeds (Huang et al., 2017), and the  
175 winter wind speed was lower than in summer. The hourly count of amine-containing  
176 particles was mostly ten times higher in winter than summer.

177 Good correlations between the hourly number count and peak area were observed in the  
178 temporal trends of DEA- ( $R^2 = 0.86$ ) and DPA-containing particles ( $R^2 = 0.88$ ) in winter.  
179 No such correlation for TMA-containing particles was observed in winter ( $R^2 = 0.22$ ) or  
180 summer (Figure 2). Besides, the hourly counts between DEA- and DPA-containing  
181 particles were well correlated in both summer ( $R^2 = 0.63$ ) and winter ( $R^2 = 0.87$ ), but only  
182 weak correlation ( $R^2 = 0.25$ ) existed between DEA- and TMA-containing particles. These  
183 results suggest DEA- and DPA-containing particles were possibly from the same sources.

184 Table 2. Meteorological factors and particle counts in summer and winter.

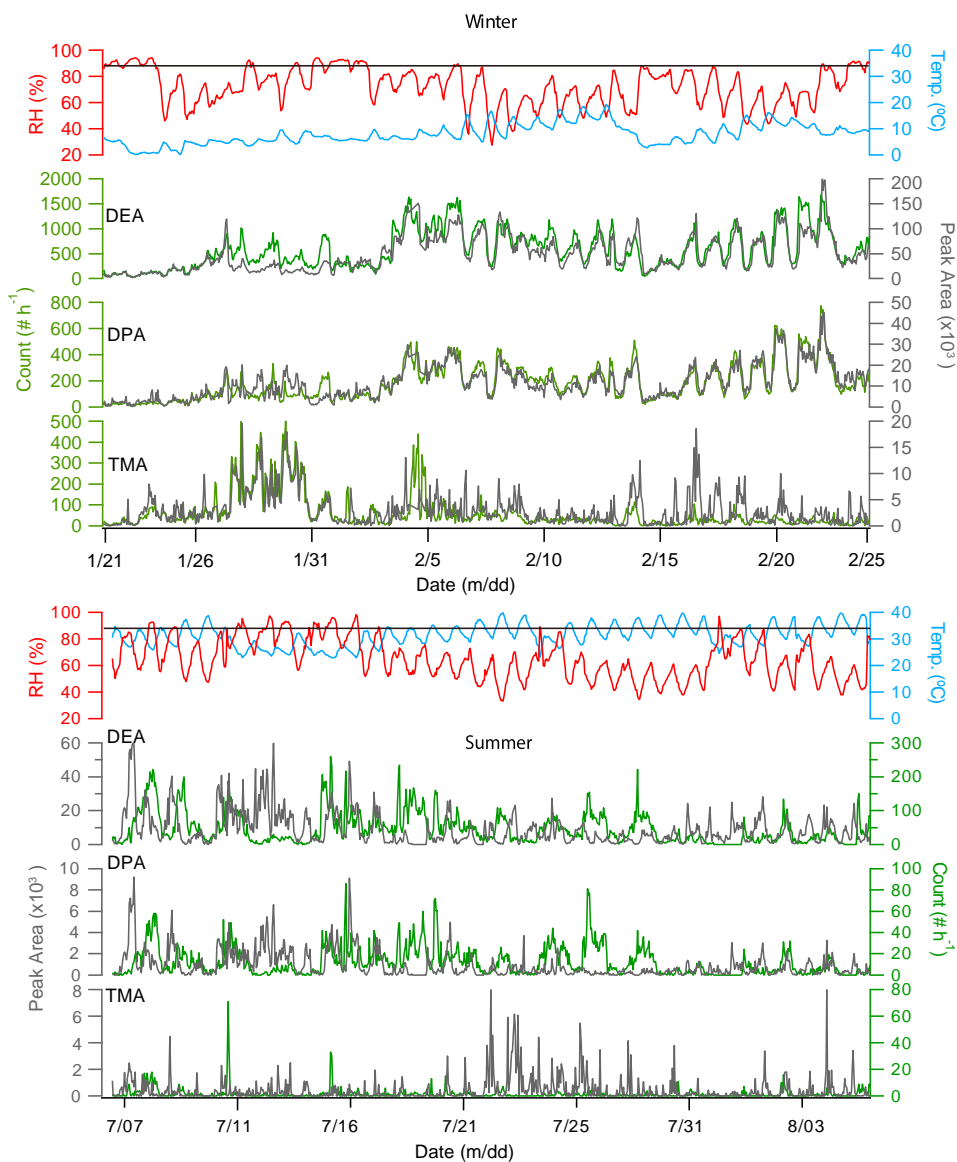
	Winter	Summer	
185			
186	Temperature (°C)	$8 \pm 4$	$31 \pm 4$
187	Relative humidity (%)	$70 \pm 14$	$64 \pm 16$
188	Wind Speed	$1.2 \pm 0.7$	$1.5 \pm 1.0$
	Amin-particle Count ( $\# \text{ h}^{-1}$ )	$587 \pm 384$	$47 \pm 26$



189 DEA- and DPA-containing particles remained at low levels from 1/20/2016 to 01/26/2016  
190 and averaged at 109 and 26 count h<sup>-1</sup>, respectively. During this period, wind speed was  
191 relatively high, commonly above 1.5 ms<sup>-1</sup>. TMA-, DEA-, and DPA-containing particles  
192 started accumulating after 01/26/2016 when wind speed was low (0.8 ms<sup>-1</sup>) and wind  
193 direction from the northwest. After 02/03/2016, DEA- and DPA-containing particles  
194 showed regular diurnal patterns with high levels of hourly count during the most daytime  
195 and a minimum level at 15:00. A similar diurnal pattern was also observed for DPA-  
196 containing particles during wintertime (Figures 3a and 3b). TMA-containing particles  
197 presented a complex diurnal profile with peaks in the early morning (4:00), at noon (12:00)  
198 and in the afternoon (18:00). The chemical composition and diurnal pattern of TMA-  
199 containing particles were strongly connected to traffic emissions.

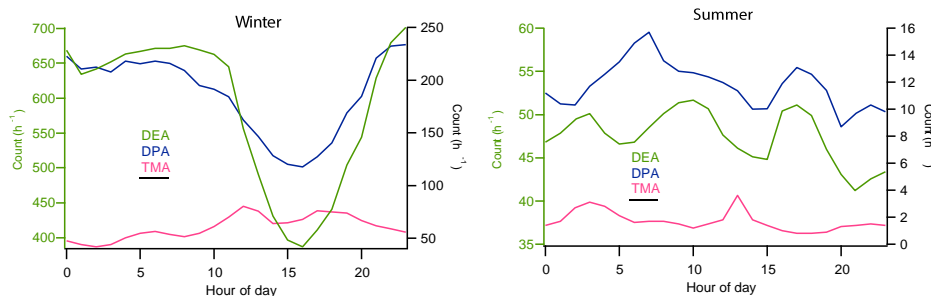
200 Wind direction and number count of amine-containing particles were analyzed together  
201 using bivariant polar plots (Figure 4). During wintertime, the dominant origin for amine-  
202 containing particles was from the northwest where a forest park was located. After being  
203 emitted from vegetation (plants, grass, and trees) (Norton, 1985), DEA partitioned to the  
204 pre-existing particles. These particles were transported to the sampling site, causing the  
205 elevation in the morning. Based on the excellent correlation between DEA- and DPA-  
206 containing particles, DPA-containing particles could also be from vegetation. It can be  
207 concluded that vegetation was the major source of amines in DEA- and DPA-containing  
208 particles from the northwest.

209



210

211 Figure 2. Temporal trends of relative humidity (RH), temperature (Temp.), hourly peak  
212 area (dark gray), and particle count (green) of DEA (m/z 74), DPA (m/z 86), and TMA  
213 (m/z 59)-containing particles in winter (top panel) and summer (bottom panel). The black  
214 lines in two panels indicate RH of 90%.



215

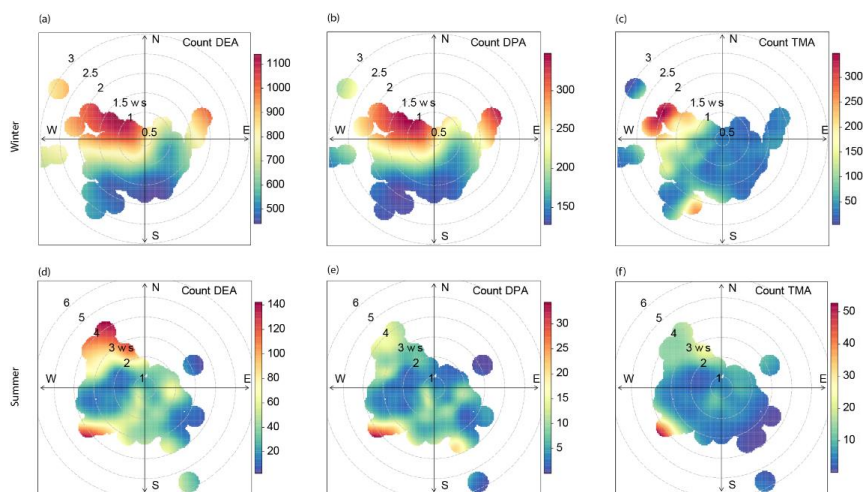
216 Figure 3. Diurnal profiles of amine-containing particles during both winter (left panel) and  
217 summer (right panel). The green left axis in each panel indicates the average number count  
218 of DEA-containing particles, while the right-axis represents the number count of both  
219 DPA- and TMA-containing particles.

220 During summer, the amine particles appeared in several episodes; each episode lasted for  
221 1~3 days. In these episodes, DPA-containing particles had two rush-hour peaks (7:00 and  
222 17:00), likely because they were also produced from traffic (Dall'Osto et al., 2016); besides  
223 the vegetation is a source of DPA-containing particles (from the southwest, Figure 4e). The  
224 DPA-containing particles peaked  $0.84 \mu\text{m}$ , suggesting that they were not freshly-emitted  
225 and had undergone substantial aging processes.

226 In summer, DEA-containing particles had a diurnal pattern of three peaks appearing at 3:00,  
227 9:00 and 17:00. TMA-containing particles had an early morning (4:00) and a noon peak  
228 (12:00). The morning peaks of DEA- and TMA-containing particles could be due to the  
229 local traffic activities, specifically, the heavy-duty vehicles which were only allowed to  
230 enter the urban area between 00:00-6:00 (Chen et al., 2017b). The polar plot showed that  
231 DEA-containing particles were from the northwest and southwest, passing through the  
232 forest park and traffic hub, respectively. This scenario seemed to be inconsistent with the



233 wintertime results because the traffic contributed limitedly in winter. In addition, due to  
234 the competition between vegetation and traffic, number count, and peak area of all the three  
235 amine-containing particles were poorly correlated with each other in summer.



236

237 Figure 4. Polar plots of the count of amine-containing particles during winter- and  
238 summertime. The circles in each figure indicate wind speed (ws).

### 239 3.3 Effect of RH on the enrichment of DEA-containing particles

240 DEA-containing particles were predominant in both winter and summer, providing a  
241 unique opportunity for investigating DEA processing. Indeed, this kind of discussion  
242 should be treated cautiously and the influences of wind speed, wind direction, temperature,  
243 and planetary boundary layer reduction should be removed. As described above, average  
244 wind speed in both winter and summer was  $1.2 \text{ ms}^{-1}$  and  $1.5 \text{ ms}^{-1}$ , respectively. In these  
245 stagnant air conditions, the sampled particles were generally local. Temperature could  
246 influence the gas-particle phase partitioning. Assuming the Henry's Law constants ( $K_H$ ) and



247 the enthalpy change  $\Delta_r H_o(K_H)$  of DEA are constant, a variation of 10°C in both summer  
248 and winter could negligibly influence the partitioning of amines from the gas phase to the  
249 particle phase, according to the Clapeyron equation (Ge et al., 2011b). In addition, the shift  
250 of planetary boundary layer (PBL) height could affect the number count and concentration  
251 of PM. The relative peak area (RPA) is defined as the peak area of each m/z divided by the  
252 total dual-ion mass spectral peak areas in a settled time bin (typically one hour) (Healy et  
253 al., 2013). Using the temporal trends of RPA can remove the influence of PBL height  
254 because it only shows the relative changes between different species which are  
255 simultaneously influenced by the shift of PBL height.

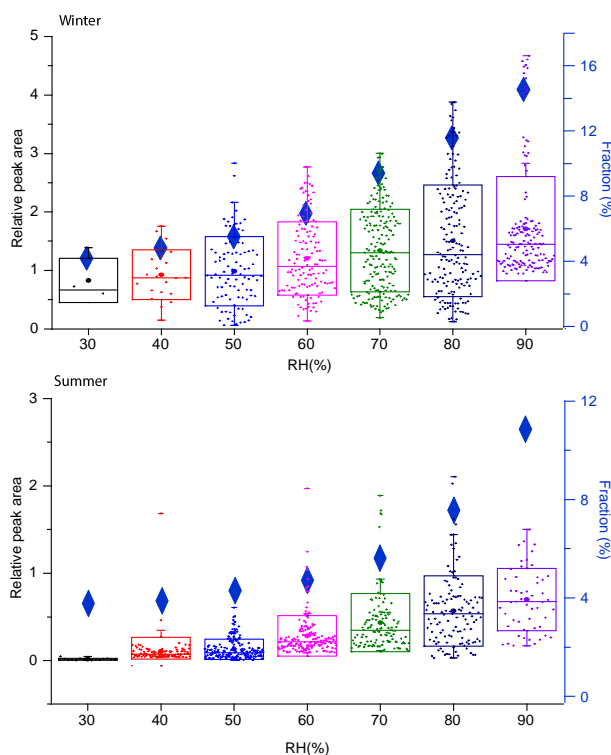
256 Box plots of DEA relative peak area under different RH conditions are shown in Figure 5.  
257 In winter, the median RPA of amine-containing particles increased by two times when RH  
258 increased from 35% to 95%. Meanwhile, the fraction of DEA-containing particles  
259 increased from 4.0% to 16.6%. In summer, the average RPA of DEA increased by three  
260 times (from 0.25 to 0.75) and the fraction of DEA-containing particles ramped from 3.8%  
261 to 12.1% when RH increased from 60% to 90%. These results suggest that RH is important  
262 for the enrichment of DEA in the particle phase. DEA was favorable to form DEA salts  
263 when reacting with HCl, H<sub>2</sub>SO<sub>4</sub>, and HNO<sub>3</sub>, and these salts had good solubility in water,  
264 making them easy to enter the aerosol phase. Along with the influence of aerosol water  
265 content, Ge et al. (2011a) also proposed that strong aerosol acidity could also enhance the  
266 partitioning of DEA in the aqueous phase. In this study, the relative acidity of amine-  
267 containing particles ((sulfate + nitrate)/ammonium, (Yao et al., 2011)) was in a range of 20-  
268 150, providing favorable conditions for the dissolution of DEA. Indeed, due to the nature  
269 of SPAMS, the amount of aerosol water content and pH were unavailable, making it





270 difficult for further analysis. Overall, these results imply that high RH condition in  
271 Chongqing was favorable for DEA to go uptake on particles, and the formed aminium salts  
272 which stabilized pre-existing particles and increased their number concentrations.

273 Rehbein et al. (2011) and Zhang et al. (2012) observed direct links between fog processing  
274 and the enhance of TMA-containing particles. High RH conditions were favorable for  
275 TMA entering the particle phase via gas-to-particle partitioning (Rehbein et al., 2011;  
276 Zhang et al., 2012). Ge et al. (2011b) argue that TMA in the aerosol phase was in the form  
277 of free base, e.g., amine, not aminium salt; TMA could be dissolved in the aerosol water  
278 content; the formation of TMA-HSO<sub>4</sub> salt was possible, but the formation of TMA-NO<sub>3</sub>  
279 and TMA-Cl was impossible due to the competition of ammonia. Thus, TMA could enter  
280 the aerosol phase by gas-aqueous partitioning, or in the form of TMA-HSO<sub>4</sub> salt. The  
281 mechanism of DEA entering the aerosol phase might be different from TMA. DEA salts  
282 were easy to form (Ge et al., 2011b). Besides, Pankow (2015) proposed that the absorptive  
283 uptake of atmospheric amines could also be possible on organic aerosols. In the context of  
284 single particle mixing state, the amine-containing particles were internally mixed with  
285 hygroscopic species, e.g., sulfate and nitrate, POA species (C<sub>x</sub>H<sub>y</sub><sup>+</sup>, see section 3.4), and  
286 SOA species (oxalate, C<sub>2</sub>H<sub>3</sub>O<sup>+</sup>). Therefore, the mixing state of amine-containing particles  
287 was also favorable for the uptake of amines via different pathways: the aqueous dissolution  
288 of aminium salts, absorptive uptake on POA and SOA.



289

290 Figure 5. Box plots of the hourly relative peak area of DEA under different RH conditions  
291 in winter (top panel) and summer (bottom panel). The boxes indicate the 25<sup>th</sup> and 75<sup>th</sup>  
292 percentiles; the dots indicate mean value with each data point representing a datum of RPA  
293 in an hour size bin. Right axis in each panel and the blue diamond show the average number  
294 fraction of amine-containing particles among the whole SPMAS dataset.

### 295 3.4 Particle types of amine-containing particles

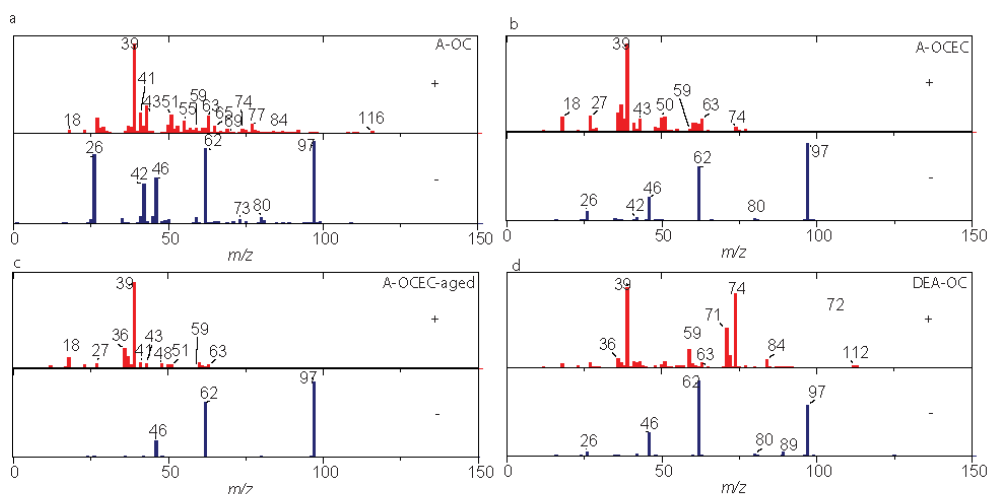
296 As shown in Figure 6, four types of amine-containing particle types were resolved,  
297 including amine-OC (A-OC, 41%), A-ECOC (39%), DEA-OC (11%), and A-ECOC-aged  
298 (9%). All these particle types had strong signals of amines, and the amines were internally  
299 mixed with sulfate, nitrate, elemental carbon, and organics.



300 In the A-OC particles, the amines were present with aromatic hydrocarbon fragments, such  
301 as  $C_4H_3^+$  ( $m/z$  51),  $C_5H_3^+$  ( $m/z$  63),  $C_6H_5^+$  ( $m/z$  77), and  $C_9H_8^+$  ( $m/z$  116), as well as with  
302 alkanes fragments such as  $C_4H_7^+$  ( $m/z$  55),  $C_4H_9^+$  ( $m/z$  57), and  $C_5H_9^+$  ( $m/z$  69). In the  
303 negative mass spectrum of A-OC, strong signals from  $CN^-$  ( $m/z$  -26) and  $CNO^-$  ( $m/z$  -42)  
304 were typically primary species, along with levoglucosan (Silva et al., 1999). The amine  
305 fragments, such as TMA ( $m/z$  59), DEA ( $m/z$  74), and DPA ( $m/z$  86) were well abundant  
306 in this particle type (76%, 95%, and 88%, respectively). The parent particles of A-OC was  
307 a kind of OC particles from biomass burning; then they mixed with amines via uptake.  
308 Meanwhile, A-OC could also be hydrophilic due to the presence of sulfate and nitrate,  
309 which could turn the particle into the water phase, making it possible for the dissolution of  
310 amines.

311 In A-ECOC mass spectra, strong signals of amines ( $m/z$  59 and 74), along with the major  
312 aromatic hydrocarbon fragments mentioned above were detected. In the negative mass  
313 spectra, nitrate and sulfate were also dominant. The A-ECOC-aged particle type had a  
314 similar chemical composition to A-ECOC ( $R^2 = 0.53$ ) but with the weaker relative  
315 intensities of  $C_xH_y^+$  and amine ions, suggesting it could be more secondary.

316 In the positive mass spectra of DEA-OC, DEA fragment ( $m/z$  74) was dominating and  
317 presenting with organic fragments described above. The secondary organic marker ions,  
318 such as  $m/z$  43 ( $[C_2H_3O]^+$ ) and -89 (oxalic acid) were found in the mass spectra. Besides,  
319 DEA-OC is not sensitive to wind speed ( $R^2 = 0.18$ ), implying they were local.



320

321 Figure 6. Average mass spectra of major particle types clustered from amine-containing  
322 particles.

323 The summertime amine-containing particles were similar to the particle types during winter  
324 (all  $R^2 > 0.7$ ) except that a Ca-rich particle type was also resolved (Figure S4). A-Ca-OC  
325 particle type was majorly composed of Calcium ( $\text{Ca}^+$  and  $\text{CaO}^+$ ), potassium ( $m/z$  23), TMA  
326 ( $m/z$  59), sulfate, nitrate, and phosphate. The A-Ca-OC particle type was from traffic  
327 activities (Chen et al., 2017a).

328 The amine-containing particle types reported in this study were different from those in  
329 literature. Cheng et al. (2018) reported that  $m/z$  74 amine-containing particles were most  
330 abundant in the Pearl River Delta, China, but the chemical composition and mixing state  
331 of amine particles were different from the present study. For example, the mixing ratio of  
332 DPA was much stronger ( $\sim 0.2$ ) than in this study ( $< 0.1$ ). In most related studies, TMA-  
333 containing particles were dominant while the present study showed DEA-containing



334 particles were dominant (Rehbein et al., 2011; Zhang et al., 2012; Healy et al., 2015; Dall  
335 et al., 2016).

#### 336 4. Conclusions

337 The amine-containing particles were analyzed using a SPAMS during winter and summer  
338 in the urban area of Chongqing. Generally, amine-containing particles were more abundant  
339 in winter than in summer. DEA-containing particles ( $m/z$  74) were the most important  
340 particle type during two observation periods. The amine-containing particles were mostly  
341 from vegetation located southwest of the sampling area. An enrichment of DEA-containing  
342 particles under high RH conditions was revealed. Amines were commonly mixed with  
343 elemental carbon, organics, sulfate, and nitrate. The amine-containing particles  
344 substantially aged during the transport. Reduction of anthropogenic amines such as DEA  
345 and TMA would improve the air quality in this region, which can be achieved by decreasing  
346 emissions of the on-road fuel-powered automobiles.

347 Acknowledgments. Financial support from the Nature Science Foundation of China (Grant  
348 No. 41375123), the National Key Research and Development Program of China  
349 (2016YFC0201506 and 2018YFC0200403), and the Starting-up project for Ph.D.  
350 (15ZA0213) are acknowledged.

351 Author Contribution. CY and YF designed the experiments; TM, SG, PC, WH, and WQ  
352 carried them out; HR, CY, ZL, CJ, and GD analyzed the experiment data; CY prepared the  
353 manuscript with contributions from all co-authors.



354 **References**

355 Angelino, S., Suess, D. T., and Prather, K. A.: Formation of aerosol particles from reactions  
356 of secondary and tertiary alkylamines: characterization by aerosol time-of-flight mass  
357 spectrometry, *Environ. Sci. Technol.*, 35, 3130-3138, 10.1021/es0015444, 2001.

358 Bzdek, B. R., Zordan, C. A., Pennington, M. R., Luther, G. W., 3rd, and Johnston, M. V.:  
359 Quantitative assessment of the sulfuric acid contribution to new particle growth, *Environ.*  
360 *Sci. Technol.*, 46, 4365-4373, 10.1021/es204556c, 2012.

361 Carslaw, D. C., Beevers, S. D., Ropkins, K., and Bell, M. C.: Detecting and quantifying  
362 aircraft and other on-airport contributions to ambient nitrogen oxides in the vicinity of a  
363 large international airport, *Atmos Environ*, 40, 5424-5434,  
364 10.1016/j.atmosenv.2006.04.062, 2006.

365 Chen, Y., Cao, J., Huang, R., Yang, F., Wang, Q., and Wang, Y.: Characterization, mixing  
366 state, and evolution of urban single particles in Xi'an (China) during wintertime haze days,  
367 *Sci. Total Environ.*, 573, 937-945, 10.1016/j.scitotenv.2016.08.151, 2016.

368 Chen, Y., Yang, F., Mi, T., Cao, J., Shi, G., Huang, R., Wang, H., Chen, J., Lou, S., and  
369 Wang, Q.: Characterizing the composition and evolution of and urban particles in  
370 Chongqing (China) during summertime, *Atmos. Res.*, 187, 84-94,  
371 10.1016/j.atmosres.2016.12.005, 2017a.

372 Chen, Y., Yang, F. M., Mi, T., Cao, J. J., Shi, G. M., Huang, R. J., Wang, H. B., Chen, J.,  
373 Lou, S. R., and Wang, Q. Y.: Characterizing the composition and evolution of and urban  
374 particles in Chongqing (China) during summertime, *Atmos. Res.*, 187, 84-94,  
375 10.1016/j.atmosres.2016.12.005, 2017b.



- 376 Cheng, C. L., Huang, Z. Z., Chan, C. K., Chu, Y. X., Li, M., Zhang, T., Ou, Y. B., Chen,  
377 D. H., Cheng, P., Li, L., Gao, W., Huang, Z. X., Huang, B., Fu, Z., and Zhou, Z.:  
378 Characteristics and mixing state of amine-containing particles at a rural site in the Pearl  
379 River Delta, China, *Atmos. Chem. Phys.*, 18, 9147-9159, 10.5194/acp-18-9147-2018, 2018.
- 380 Dall'Osto, M., Beddows, D. C. S., McGillicuddy, E. J., Esser-Gietl, J. K., Harrison, R. M.,  
381 and Wenger, J. C.: On the simultaneous deployment of two single-particle mass  
382 spectrometers at an urban background and a roadside site during SAPUSS, *Atmos. Chem.*  
383 *Phys.*, 16, 9693-9710, 10.5194/acp-16-9693-2016, 2016.
- 384 Dall, apos, Osto, M., Beddows, D. C. S., McGillicuddy, E. J., Esser-Gietl, J. K., Harrison,  
385 R. M., and Wenger, J. C.: On the simultaneous deployment of two single-particle mass  
386 spectrometers at an urban background and a roadside site during SAPUSS, *Atmos. Chem.*  
387 *Phys.*, 16, 9693-9710, 10.5194/acp-16-9693-2016, 2016.
- 388 Dallosto, M., and Harrison, R.: Chemical characterisation of single airborne particles in  
389 Athens (Greece) by ATOFMS, *Atmos. Environ.*, 40, 7614-7631,  
390 10.1016/j.atmosenv.2006.06.053, 2006.
- 391 De Haan, D. O., Hawkins, L. N., Kononenko, J. A., Turley, J. J., Corrigan, A. L., Tolbert,  
392 M. A., and Jimenez, J. L.: Formation of nitrogen-containing oligomers by methylglyoxal  
393 and amines in simulated evaporating cloud droplets, *Environ. Sci. Technol.*, 45, 984-991,  
394 10.1021/es102933x, 2011.
- 395 Denkenberger, K. A., Moffet, R. C., Holecek, J. C., Rebotier, T. P., and Prather, K. A.:  
396 Real-time, single-particle measurements of oligomers in aged ambient aerosol particles,  
397 *Environ. Sci. Technol.*, 41, 5439-5446, 10.1021/es070329l, 2007.



- 398 Ge, X., Wexler, A. S., and Clegg, S. L.: Atmospheric amines – Part I. A review, Atmos.  
399 Environ., 45, 524-546, [10.1016/j.atmosenv.2010.10.012](https://doi.org/10.1016/j.atmosenv.2010.10.012), 2011a.
- 400 Ge, X., Wexler, A. S., and Clegg, S. L.: Atmospheric amines – Part II. Thermodynamic  
401 properties and gas/particle partitioning, Atmos. Environ., 45, 561-577,  
402 <https://doi.org/10.1016/j.atmosenv.2010.10.013>, 2011b.
- 403 Gómez Alvarez, E., Viidanoja, J., Muñoz, A., Wirtz, K., and Hjorth, J.: Experimental  
404 Confirmation of the Dicarbonyl Route in the Photo-oxidation of Toluene and Benzene,  
405 Environ. Sci. Technol., 41, 8362-8369, [10.1021/es0713274](https://doi.org/10.1021/es0713274), 2007.
- 406 Healy, R. M., Sciare, J., Poulain, L., Crippa, M., Wiedensohler, A., Prévôt, A. S.,  
407 Baltensperger, U., Sarda-Estève, R., McGuire, M. L., and Jeong, C.-H.: Quantitative  
408 determination of carbonaceous particle mixing state in Paris using single-particle mass  
409 spectrometer and aerosol mass spectrometer measurements, Atmos. Chem. Phys., 13,  
410 9479-9496, 2013.
- 411 Healy, R. M., Evans, G. J., Murphy, M., Sierau, B., Arndt, J., McGillicuddy, E., O'Connor,  
412 I. P., Sodeau, J. R., and Wenger, J. C.: Single-particle speciation of alkylamines in ambient  
413 aerosol at five European sites, Anal Bioanal Chem, 407, 5899-5909, [10.1007/s00216-014-](https://doi.org/10.1007/s00216-014-8092-1)  
414 [8092-1](https://doi.org/10.1007/s00216-014-8092-1), 2015.
- 415 Huang, Q., Cai, X., Song, Y., and Zhu, T.: Air stagnation in China (1985–2014):  
416 climatological mean features and trends, Atmos. Chem. Phys., 17, 7793-7805,  
417 [10.5194/acp-17-7793-2017](https://doi.org/10.5194/acp-17-7793-2017), 2017.





- 418 Huang, Y. L., Chen, H., Wang, L., Yang, X., and Chen, J. M.: Single particle analysis of  
419 amines in ambient aerosol in Shanghai, *Environ Chem*, 9, 202-210, 10.1071/En11145,  
420 2012.
- 421 Kirkby, J., Curtius, J., Almeida, J., Dunne, E., Duplissy, J., Ehrhart, S., Franchin, A., Gagne,  
422 S., Ickes, L., Kurten, A., Kupc, A., Metzger, A., Riccobono, F., Rondo, L., Schobesberger,  
423 S., Tsagkogeorgas, G., Wimmer, D., Amorim, A., Bianchi, F., Breitenlechner, M., David,  
424 A., Dommen, J., Downard, A., Ehn, M., Flagan, R. C., Haider, S., Hansel, A., Hauser, D.,  
425 Jud, W., Junninen, H., Kreissl, F., Kvashin, A., Laaksonen, A., Lehtipalo, K., Lima, J.,  
426 Lovejoy, E. R., Makhmutov, V., Mathot, S., Mikkila, J., Minginette, P., Mogo, S.,  
427 Nieminen, T., Onnela, A., Pereira, P., Petaja, T., Schnitzhofer, R., Seinfeld, J. H., Sipila,  
428 M., Stozhkov, Y., Stratmann, F., Tome, A., Vanhanen, J., Viisanen, Y., Vrtala, A., Wagner,  
429 P. E., Walther, H., Weingartner, E., Wex, H., Winkler, P. M., Carslaw, K. S., Worsnop, D.  
430 R., Baltensperger, U., and Kulmala, M.: Role of sulphuric acid, ammonia and galactic  
431 cosmic rays in atmospheric aerosol nucleation, *Nature*, 476, 429-433, 10.1038/nature10343,  
432 2011.
- 433 Li, L., Huang, Z., Dong, J., Li, M., Gao, W., Nian, H., Fu, Z., Zhang, G., Bi, X., Cheng, P.,  
434 and Zhou, Z.: Real time bipolar time-of-flight mass spectrometer for analyzing single  
435 aerosol particles, *Int. J. Mass spectrom.*, 303, 118-124, 10.1016/j.ijms.2011.01.017, 2011.
- 436 Moffet, R. C., de Foy, B., Molina, L. T., Molina, M. J., and Prather, K. A.: Measurement  
437 of ambient aerosols in northern Mexico City by single particle mass spectrometry, *Atmos.*  
438 *Chem. Phys.*, 8, 4499-4516, 10.5194/acp-8-4499-2008, 2008.



- 439 Monks, P. S.: Gas-phase radical chemistry in the troposphere, *Chem. Soc. Rev.*, 34, 376-  
440 395, [10.1039/b307982c](https://doi.org/10.1039/b307982c), 2005.
- 441 Norton, R.: Observation of diethylamine in tropospheric aerosols, *Eos, Transactions,*  
442 *American Geophysical Union*, 66, 823-823, 1985.
- 443 Onasch, T. B., Trimborn, a., Fortner, E. C., Jayne, J. T., Kok, G. L., Williams, L. R.,  
444 Davidovits, P., and Worsnop, D. R.: Soot Particle Aerosol Mass Spectrometer:  
445 Development, Validation, and Initial Application, *Aerosol Sci. Technol.*, 46, 804-817,  
446 [10.1080/02786826.2012.663948](https://doi.org/10.1080/02786826.2012.663948), 2012.
- 447 Pankow, J. F.: Phase considerations in the gas/particle partitioning of organic amines in the  
448 atmosphere, *Atmos. Environ.*, 122, 448-453,  
449 <https://doi.org/10.1016/j.atmosenv.2015.09.056>, 2015.
- 450 Pratt, K. A., Murphy, S. M., Subramanian, R., DeMott, P. J., Kok, G. L., Campos, T.,  
451 Rogers, D. C., Prenni, A. J., Heymsfield, A. J., Seinfeld, J. H., and Prather, K. A.: Flight-  
452 based chemical characterization of biomass burning aerosols within two prescribed burn  
453 smoke plumes, *Atmos. Chem. Phys.*, 11, 12549-12565, [10.5194/acp-11-12549-2011](https://doi.org/10.5194/acp-11-12549-2011), 2011.
- 454 Qin, X., Pratt, K. A., Shields, L. G., Toner, S. M., and Prather, K. A.: Seasonal comparisons  
455 of single-particle chemical mixing state in Riverside, CA, *Atmos. Environ.*, 59, 587-596,  
456 [10.1016/j.atmosenv.2012.05.032](https://doi.org/10.1016/j.atmosenv.2012.05.032), 2012.
- 457 Rehbein, P. J., Jeong, C. H., McGuire, M. L., Yao, X., Corbin, J. C., and Evans, G. J.:  
458 Cloud and fog processing enhanced gas-to-particle partitioning of trimethylamine, *Environ.*  
459 *Sci. Technol.*, 45, 4346-4352, [10.1021/es1042113](https://doi.org/10.1021/es1042113), 2011.



- 460 Silva, P. J., Liu, D.-Y., Noble, C. A., and Prather, K. A.: Size and Chemical  
461 Characterization of Individual Particles Resulting from Biomass Burning of Local  
462 Southern California Species, *Environ. Sci. Technol.*, 33, 3068-3076, 10.1021/es980544p,  
463 1999.
- 464 Smith, J. N., Barsanti, K. C., Friedli, H. R., Ehn, M., Kulmala, M., Collins, D. R.,  
465 Scheckman, J. H., Williams, B. J., and McMurry, P. H.: Observations of ammonium salts in  
466 atmospheric nanoparticles and possible climatic implications, *Proc Natl Acad Sci U S A*,  
467 107, 6634-6639, 10.1073/pnas.0912127107, 2010.
- 468 Song, X.-H., Hopke, P. K., Fergenson, D. P., and Prather, K. A.: Classification of Single  
469 Particles Analyzed by ATOFMS Using an Artificial Neural Network, ART-2A, *Anal.*  
470 *Chem.*, 71, 860-865, 10.1021/ac9809682, 1999.
- 471 Tan, P. V., Evans, G. J., Tsai, J., Owega, S., Fila, M. S., Malpica, O., and Brook, J. R.: On-  
472 line analysis of urban particulate matter focusing on elevated wintertime aerosol  
473 concentrations, *Environ. Sci. Technol.*, 36, 3512-3518, 10.1021/es011448i, 2002.
- 474 Tao, J., Zhang, L., Cao, J., and Zhang, R.: A review of current knowledge concerning  
475  $PM_{2.5}$ ; chemical composition, aerosol optical properties and their  
476 relationships across China, *Atmos. Chem. Phys.*, 17, 9485-9518, 10.5194/acp-17-9485-  
477 2017, 2017.
- 478 Wang, J., Ge, X., Chen, Y., Shen, Y., Zhang, Q., Sun, Y., Xu, J., Ge, S., Yu, H., and Chen,  
479 M.: Highly time-resolved urban aerosol characteristics during springtime in Yangtze River  
480 Delta, China: insights from soot particle aerosol mass spectrometry, *Atmos. Chem. Phys.*,  
481 16, 9109-9127, 10.5194/acp-16-9109-2016, 2016.



- 482 Wang, L., Khalizov, A. F., Zheng, J., Xu, W., Ma, Y., Lal, V., and Zhang, R.: Atmospheric  
483 nanoparticles formed from heterogeneous reactions of organics, *Nature Geoscience*, 3, 238,  
484 [10.1038/ngeo778](https://doi.org/10.1038/ngeo778)  
485 <https://www.nature.com/articles/ngeo778#supplementary-information>, 2010.
- 486 Yao, L., Garmash, O., Bianchi, F., Zheng, J., Yan, C., Kontkanen, J., Junninen, H., Mazon,  
487 S. B., Ehn, M., Paasonen, P., Sipila, M., Wang, M., Wang, X., Xiao, S., Chen, H., Lu, Y.,  
488 Zhang, B., Wang, D., Fu, Q., Geng, F., Li, L., Wang, H., Qiao, L., Yang, X., Chen, J.,  
489 Kerminen, V. M., Petaja, T., Worsnop, D. R., Kulmala, M., and Wang, L.: Atmospheric  
490 new particle formation from sulfuric acid and amines in a Chinese megacity, *Science*, 361,  
491 278-281, [10.1126/science.aao4839](https://doi.org/10.1126/science.aao4839), 2018.
- 492 Yao, X., Rehbein, P. J. G., Lee, C. J., Evans, G. J., Corbin, J., and Jeong, C.-H.: A study  
493 on the extent of neutralization of sulphate aerosol through laboratory and field experiments  
494 using an ATOFMS and a GPIC, *Atmos. Environ.*, 45, 6251-6256,  
495 [10.1016/j.atmosenv.2011.06.061](https://doi.org/10.1016/j.atmosenv.2011.06.061), 2011.
- 496 You, Y., Kanawade, V. P., de Gouw, J. A., Guenther, A. B., Madronich, S., Sierra-  
497 Hernández, M. R., Lawler, M., Smith, J. N., Takahama, S., Ruggeri, G., Koss, A., Olson,  
498 K., Baumann, K., Weber, R. J., Nenes, A., Guo, H., Edgerton, E. S., Porcelli, L., Brune,  
499 W. H., Goldstein, A. H., and Lee, S. H.: Atmospheric amines and ammonia measured with  
500 a chemical ionization mass spectrometer (CIMS), *Atmos. Chem. Phys.*, 14, 12181-12194,  
501 [10.5194/acp-14-12181-2014](https://doi.org/10.5194/acp-14-12181-2014), 2014.
- 502 Zhang, G., Bi, X., Chan, L. Y., Li, L., Wang, X., Feng, J., Sheng, G., Fu, J., Li, M., and  
503 Zhou, Z.: Enhanced trimethylamine-containing particles during fog events detected by



504 single particle aerosol mass spectrometry in urban Guangzhou, China, Atmos. Environ.,

505 55, 121-126, 10.1016/j.atmosenv.2012.03.038, 2012.

506